Book Chapter

A Computational DFT Study of the Stereoinversion of Succinimide Residues Formed in Proteins and Peptides Catalyzed by a Hydrogen Phosphate Ion: An Unsymmetrical S_E1 Mechanism

Ohgi Takahashi

Faculty of Pharmaceutical Sciences, Shonan University of Medical Sciences, 16-10 Kamishinano, Totsuka-ku, Yokohama 244-0806, Japan

***Corresponding Author: Ohgi Takahashi,** Faculty of Pharmaceutical Sciences, Shonan University of Medical Sciences, 16-10 Kamishinano, Totsuka-ku, Yokohama 244-0806, Japan

Published **January 09, 2025**

This Book Chapter is a republication of an article published by Ohgi Takahashi at Symmetry in October 2024. (Takahashi, O. A Computational DFT Study of the Stereoinversion of Succinimide Residues Formed in Proteins and Peptides Catalyzed by a Hydrogen Phosphate Ion: An Unsymmetrical S_E1 Mechanism. Symmetry 2024, 16, 1369. https://doi.org/10.3390/sym16101369)

How to cite this book chapter: Ohgi Takahashi. A Computational DFT Study of the Stereoinversion of Succinimide Residues Formed in Proteins and Peptides Catalyzed by a Hydrogen Phosphate Ion: An Unsymmetrical S_E1 Mechanism. Top 10 Contributions in Symmetry. Hyderabad, India: Academic Reads. 2025.

Funding: This research was funded by Grants-in-Aid for Scientific Research (no. 22K12268) from the Japan Society for the Promotion of Science.

Data Availability Statement: The data that support the findings of this study are available in the article itself. Any additional in formation (e.g., the Cartesian coordinates of the optimized geometries) will be made available by the author on request.

Conflicts of Interest: The author declares no conflicts of interest.

Abstract

Succinimide residues formed spontaneously from aspartic acid (Asp) and asparagine (Asn) residues in proteins and peptides are stereochemically unstable, undergoing partial L-to-D stereoinversion, and this is responsible for the D-Asp and D-β-Asp residues found in long-lived proteins. These stereoinverted abnormal amino acid residues are believed to be related to aging and some age-related diseases such as cataracts. Although the succinimide stereoinversion is nonenzymatic, a catalyst is required for it to occur at physiological temperature. In this study, it was found by density functional theory (DFT) calculations that a hydrogen phosphate ion (HPO_4^{2-}) can effectively catalyze the stereoinversion of the succinimide intermediate. The HPO_4^{2-} ion abstracts a proton from the asymmetric carbon atom of the succinimide residue to form an enolate intermediate. Then, while the resultant dihydrogen phosphate ion ($H_2PO_4^-$) remains bound to the enolate ion, a water molecule donates a proton to the enolate intermediate on the opposite side from the phosphate (which is the rate-determining step) to produce the inverted carbon atom. The calculated activation barrier (ca. 90 kJ mol^{-1}) is consistent with a slow in vivo reaction. The present found mechanism can be termed the “unsymmetrical S_E1” or “pseudo-S_E2” mechanism.

Keywords

Succinimide; Stereoinversion; Nonenzymatic Reaction; Catalyst; Hydrogen Phosphate Ion; Computational Study; Density Functional Theory; Unsymmetrical S_E1 Mechanism; Pseudo-S_E2 Mechanism

1. Introduction

Various nonenzymatic reactions that occur spontaneously in proteins and peptides (especially in long-lived proteins) are believed to be related to aging and some diseases (especially age-related diseases such as cataracts and Alzheimer's disease) [1–10]. Among such reactions, there are L-to-D partial stereoinversions of amino acid residues [11–21]. Except for glycine (Gly), which is not chiral, only L-amino acids are used in protein biosynthesis. However, D-amino acid residues have been found in proteins and peptides, especially in long-lived and/or disease-related proteins and peptides. The L-to-D partial stereoinversion of an amino acid residue of proteins and peptides is often called "racemization". However, this is inadequate because the stereoinversion of an amino acid residue does not give the enantiomer but an epimer of the original molecule. In this present paper, which deals with the quantum chemical calculation of the reaction for a single molecule, I simply use the term "stereoinversion". The "partial stereoinversion" is the macroscopic outcome.

Aspartic acid (Asp) residues are unstable stereochemically. This is due to the succinimide-linked mechanism shown in Scheme 1 [22–27]. The L-Asp residue can undergo nonenzymatic and spontaneous cyclization to the five-membered ring L-succinimide intermediate with the release of a water molecule. The L-succinimide may be intramolecularly hydrolyzed back to L-Asp or to L-β-Asp. Moreover, since the succinimide residue is prone to a catalyzed stereoinversion, L-succinimide may be converted to D-succinimide, from which D-Asp and D-β-Asp residues can be produced. The formation of the unusual L-β-Asp, D-Asp, and D-β-Asp residues can affect the protein structures and functions [28–30]. Succinimide intermediates can also be formed from the asparagine (Asn) residues triggering the

reactions known as deamidation [22,23,31]. This is irreversible because of the release of an ammonia molecule. Therefore, there can be L-β-Asp, D-Asp, and D-β-Asp residues in proteins originating from Asn residues. It should be noted that the actual species that directly undergoes stereoinversion is the succinimide intermediate. In this present paper, I focus on the stereoinversion of the succinimide intermediate.

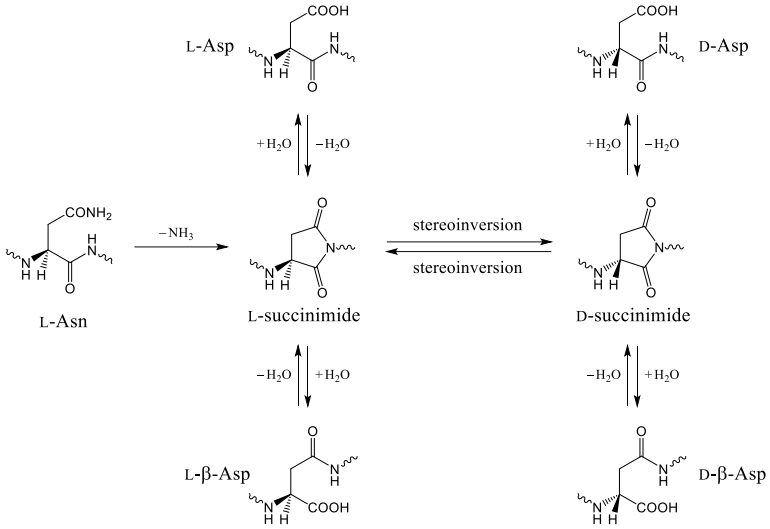

Scheme 1: The succinimide-linked nonenzymatic reactions from aspartic acid (Asp) and asparagine (Asn) residues.

Although the succinimide stereoinversion is nonenzymatic, a catalyst is required for it to occur at physiological temperature. Experimentally, however, it is hardly known what actually act as a catalyst in vivo. It was previously shown computationally that a dihydrogen phosphate ion ($H_2PO_4^-$) can be a catalyst of the succinimide stereoinversion [27]. On the other hand, the racemization of 5-phenylhydantoin, which has a five-membered ring similar to succinimide, was clearly shown to be catalyzed by a hydrogen phosphate ion (HPO_4^{2-}) rather than by $H_2PO_4^-$ in a phosphate buffer [32]. Moreover, at the physiological pH of 7.4, the ratio of HPO_4^{2-} and $H_2PO_4^-$ is about 4:1, since the pK_a of $H_2PO_4^-$ is 6.82 [33]. In the present study, I computationally searched for a mechanism by which the succinimide residue stereoinversion is catalyzed by the HPO_4^{2-} ion. The typical

activation energies of nonenzymatic reactions in peptides are less than 100 kJ mol^{-1} [8,22,25]. Using a model molecule, I extensively investigated the reaction pathways for succinimide stereoinversion and found only one reaction pathway where the activation barrier in water is less than 100 kJ mol^{-1} (ca. 90 kJ mol^{-1}), which will be reported here.

Catalysis by the HPO_4^{2-} ion can be regarded as an example of general base catalysis. Two common mechanisms have been considered for general base-catalyzed racemization: S_E1 (substitution, electrophilic, and unimolecular) and S_E2 (substitution, electrophilic, and bimolecular) [34–43]. In the S_E1 mechanism, a resonance-stabilized flat carbanion (such as an enolate ion) is formed as an intermediate. In the S_E2 mechanism, no intermediate is formed, and stereoinversion proceeds in one step. The two mechanisms have been distinguished by kinetic study in a deuterated environment. So far, most of the general base-catalyzed racemization reactions were proposed to occur by the S_E1 mechanism. In this present study, a new mechanism was found in which an enolate intermediate is formed, but the reaction can not be kinetically distinguished from the S_E2 mechanism. It is proposed that the new mechanism is termed the "unsymmetrical S_E1" or "pseudo-S_E2" mechanism.

2. Computational Method

The quantum chemical calculations in this present study were performed by using Spartan'20 [44]. Figure 1 shows the model molecule (L- or *S*-form) used as the reactant (R). In this molecule, an aminosuccinyl residue is capped by acetyl and NCH_3 groups on the N- and C-termini, respectively, in order to mimic the peptide-bound succinimide. The C_α atom is the asymmetric carbon atom (L- or *S*-configuration). Scheme 2 shows the postulated reaction mechanism. The catalytic HPO_4^{2-} ion was supposed to abstract the proton from C_α to form an enolate intermediate. In order to complete the stereoinversion, a proton has to be donated to the enolate ion on the opposite side from the phosphate. As the proton donor, a water (H_2O) molecule was explicitly included.

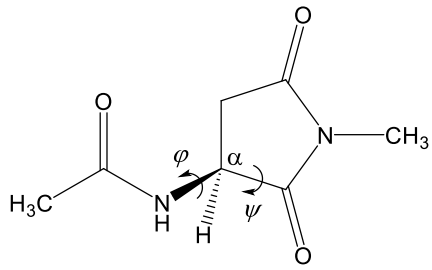

Figure 1: The model molecule used for calculation in this present study. The α carbon atom (C_α) is in the L-configuration. The symbols φ and ψ represent the C–N–C_α–C and N–C_α–C–N dihedral angles, respectively, corresponding to the main chain of the original Asp or Asn residue.

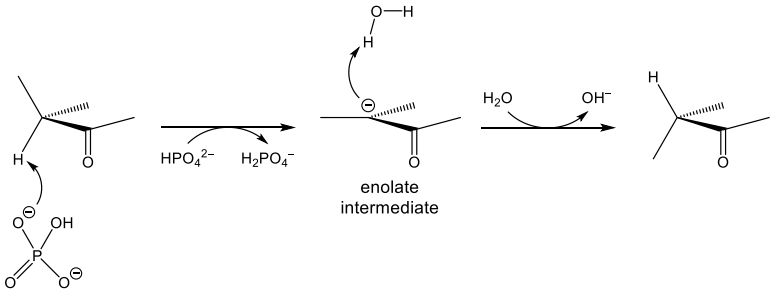

Scheme 2: A schematic representation of the postulated reaction mechanism.

The calculations were performed with the density functional theory (DFT) method with the ωB97X-D functional [45] and the 6-311+G(d,p) basis set. This present paper deals with systems having hydrogen bonds (including the CH···O type). Although hydrogen bond interactions are dominated by electrostatic interactions, it is necessary to include dispersion interactions to obtain accurate energetics. The ωB97X-D functional, which includes empirical atom–atom dispersion corrections, is known to perform well for hydrogen bond interactions [46]. Equilibrium and transition state (TS) geometries were fully optimized in water. The solvent effect of water was included by the conductor-like polarizable continuum model (C-PCM) implemented in Spartan'20 (with a dielectric constant of 78.3). By the default setting of Spartan'20, the van der Waals radii scaled by 1.2 are used in the C-PCM model. However, this scaling was not used in this present study, because a much better result is obtained with no scaling for the hydration Gibbs energy

of the HPO_4^{2-} ion. Since HPO_4^{2-} has a −2 charge, its hydration Gibbs energy is exceedingly high. Although no definitive value is available [47], Moser recommended the value of 1078 kJ mol^{-1} (298 K) based on his sophisticated analysis [48]. This value is close to the earlier estimate by Florián and Warshel [49] of 1025 kJ mol^{-1}. The hydration Gibbs energy of HPO_4^{2-} is calculated to be 1053 kJ mol^{-1} by the C-PCM model with no scaling (based on the gas phase and aqueous phase optimized geometries and the standard thermal corrections), while it is 971 kJ mol^{-1} with scaling by 1.2.

Vibrational frequency calculations were performed for the optimized geometries by a numerical differentiation of the analytical gradients to verify them as an energy minimum (no imaginary frequency) or a TS (a single imaginary frequency) and to correct the energies for the zero-point energy (ZPE). The relative energies reported hereafter are the ZPE-corrected energies. Moreover, the intrinsic reaction coordinate (IRC) calculations were performed from TSs to confirm the minima connected by each TS.

3. Results and Discussion

For the model molecule, two conformers (Figure 2) were found that have almost the same energies. These two conformers can be denoted as *anti*-periplanar and *syn*-periplanar with respect to the C_α–H_α bond and the adjacent N–H bond. In the *anti*-periplanar conformer, the H_α–C_α–N–H dihedral angle is −171° and the φ dihedral angle (Figure 1) is −106°. In the *syn*-periplanar conformer, the H_α–C_α–N–H dihedral angle is −12° and φ = 54°. The *syn*-periplanar conformer is only 0.9 kJ mol^{-1} lower than the *anti*-periplanar conformer. Here, a low-energy stereoinversion pathway from the *anti*-periplanar conformer is reported. Hereafter, the *anti*-planar conformer of the model compound in the L-form is denoted as R (reactant). The product (denoted as P) is the *syn*-periplanar conformer of the stereoinverted D-form of the model molecule. The overall energy diagram is shown in Figure 3.

anti-periplanar *syn*-periplanar

Figure 2: Two conformers of the model molecule (reactant, R): *anti*-periplanar (left; $\varphi = -106°$, $\psi = -139°$) and *syn*-periplanar (right; $\varphi = 54°$, $\psi = -139°$). The C_α atom is in the L-configuration. Grey: carbon; white: hydrogen; blue: nitrogen; and red: oxygen.

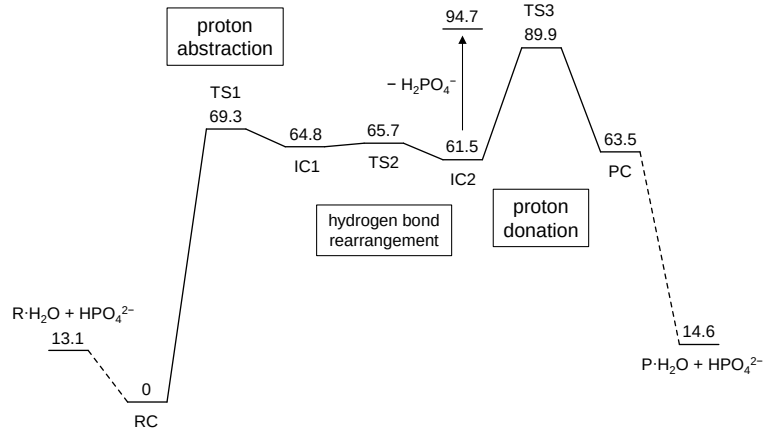

Figure 3: Energy diagram for the HPO_4^{2-}-catalyzed stereoinversion of succinimide. The ZPE-corrected relative energies in water are shown in kJ mol^{-1} (with respect to the RC). The imaginary frequencies of TS1, TS2, and TS3 are 1202i, 64i, and 1413i cm^{-1}, respectively.

The reaction starts from the reactant complex (RC) shown in Figure 4. The RC is a complex between R, an HPO_4^{2-} ion, and an H_2O molecule. In order to roughly estimate the stabilization energy of R by complexing with an HPO_4^{2-} ion in water, the geometries of the $R{\cdot}H_2O$ complex and the HPO_4^{2-} ion were separately optimized. The sum of energies of these two species was 13.1 kJ mol^{-1} higher than the RC (Figure 3).

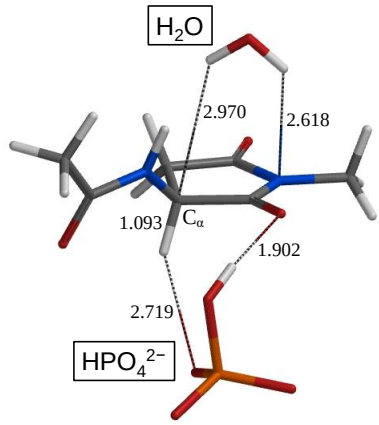

Figure 4: The geometry of the RC (reactant complex) ($\varphi = -140°$, $\psi = -137°$). Relevant interatomic distances are shown in Å. Grey: carbon; white: hydrogen; blue: nitrogen; red: oxygen; and orange: phosphorus.

From the RC, the reaction proceeds in three steps. In the first step, the HPO_4^{2-} ion abstracts a proton from the C_α atom to form an enolate intermediate (a complex with an $H_2PO_4^-$ ion and an H_2O molecule). In the second step, hydrogen bond reorganization occurs. This step is almost barrierless. In the third step, which is the rate-determining step, the H_2O molecule donates a proton to the enolate intermediate to provide the product complex (PC), which is the complex between P, an $H_2PO_4^-$ ion, and an OH^- ion. The PC is higher in energy than the sum of the separated P·H_2O complex and HPO_4^{2-} ion. The details of the reaction pathway are described below.

3.1. The First Step: Proton Abstraction

Figure 4 shows the reactant complex, RC. This is a complex between the reactant R (L-form, *anti*-periplanar), the HPO_4^{2-} ion, and an H_2O molecule. The H_α–C_α–N–H dihedral angle is 159°. The HPO_4^{2-} ion abstracts a proton from the C_α atom of R in the first step. The H_2O molecule acts as a proton donor in the third step. In the RC, the C_α–H_α bond seems to interact with an anionic oxygen atom of HPO_4^{2-} by a CH···O anionic hydrogen bond (2.719 Å). The OH group in HPO_4^{2-} also forms a hydrogen bond to a carbonyl oxygen of the succinimide moiety (1.902 Å).

The H_2O molecule seems to interact weakly with the succinimide nitrogen atom by a hydrogen bond of 2.618 Å. The distance between the C_α atom of R and a hydrogen atom of H_2O is 2.970 Å. As noted above, the association of $R{\cdot}H_2O$ with an HPO_4^{2-} ion leads to stabilization by ca. 13 kJ mol^{-1}.

TS1 (transition state 1) shown in Figure 5 is the TS of the first step. The C_α–H_α bond has been elongated, and the $C_\alpha{\cdots}H_\alpha$ distance is 1.492 Å in TS1. The distance between H_α and the phosphate oxygen atom has become very short (1.147 Å), and an $H_2PO_4^-$ ion is almost formed. The relative energy of TS1 with respect to the RC is as low as 69.3 kJ mol^{-1}.

IC1 (intermediate complex 1), shown in Figure 6, is a complex between the enolate intermediate, an $H_2PO_4^-$ ion, and an H_2O molecule and is directly connected to TS1. The C_α atom was sp^3-hybridized in the RC, but it is now sp^2-hybridized. The distance between C_α and the H atom of the newly formed phosphate O–H bond is 2.090 Å; this distance may be regarded as one of an anionic hydrogen bond. The hydrogen bond between the succinimide carbonyl oxygen and phosphate is very short (1.685 Å). The energy of IC1 is 64.8 kJ mol^{-1} relative to the RC and is lower than TS1 by 4.5 kJ mol^{-1}.

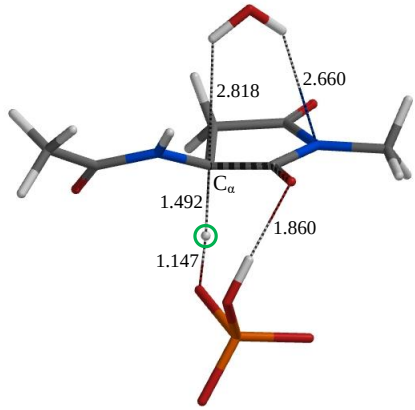

Figure 5: The geometry of TS1 (transition state 1) (φ = −163°, ψ = −150°) connecting the RC (Figure 4) and IC1 (Figure 6). Relevant interatomic distances are shown in Å. Grey: carbon; white: hydrogen; blue: nitrogen; red: oxygen; and orange: phosphorus. The transferring proton is indicated by the green circle.

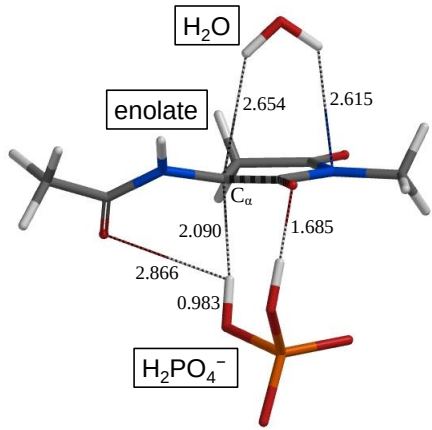

Figure 6: The geometry of IC1 (intermediate complex 1) (φ = −147°, ψ = −165°). Relevant interatomic distances are shown in Å. Grey: carbon; white: hydrogen; blue: nitrogen; red: oxygen; and orange: phosphorus.

3.2. The Second Step: Hydrogen Bond Reorganization in the Intermediate Complex

In IC1, the hydrogen atom abstracted from C_α in the first step still interacts with C_α (2.090 Å), and the distance between C_α and the water hydrogen atom is relatively long (2.654 Å). It was found that a hydrogen bond reorganization is required to occur before the H_2O molecule can donate a proton to the enolate intermediate.

TS2 (transition state 2), shown in Figure 7, is the TS of the hydrogen bond reorganization in the intermediate complex. In TS2, the anionic hydrogen bond between C_α and the phosphate is being broken (2.595 Å) and a new hydrogen bond is being created (2.318 Å) between the carbonyl oxygen of the acetyl group and the phosphate. The interaction between C_α and H_2O has become slightly shorter (2.538 Å). The energy of TS2 is only 0.9 kJ mol^{-1} higher than IC1, and the second step is almost barrierless.

IC2 (intermediate complex 2), shown in Figure 8, is directly connected to TS2. The energy of IC2 is lower than IC1 by 3.3 kJ mol^{-1} and is higher than the RC by 61.5 kJ mol^{-1}. The anionic hydrogen bond between C_α and the phosphate has been broken

(3.519 Å) in IC2. On the other hand, a new hydrogen bond has been created between the acetyl oxygen and the phosphate (1.766 Å). Moreover, the interaction between C_α and the water hydrogen atom has become considerably shorter (2.163 Å). The C_α atom is now ready to abstract a proton from the H_2O molecule. In other words, the H_2O molecule is now ready to donate a proton to the C_α atom.

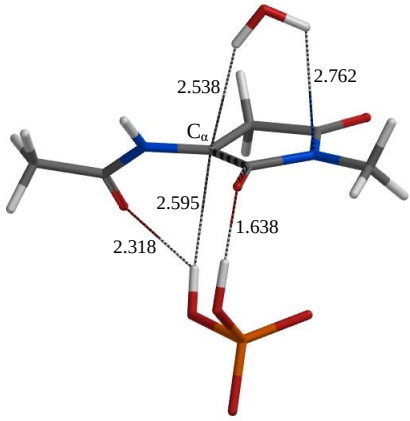

Figure 7: The geometry of TS2 (transition state 2) (φ = −132°, ψ = −171°) connecting IC1 (Figure 6) and IC2 (Figure 8). Relevant interatomic distances are shown in Å. Grey: carbon; white: hydrogen; blue: nitrogen; red: oxygen; and orange: phosphorus.

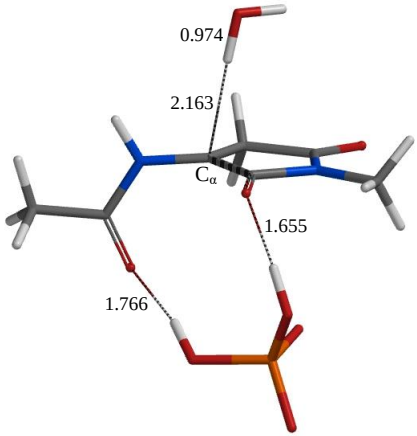

Figure 8: The geometry of IC2 (intermediate complex 2) (φ = −85°, ψ = 175°). Relevant interatomic distances are shown in Å. Grey: carbon; white: hydrogen; blue: nitrogen; red: oxygen; and orange: phosphorus.

3.3. The Third Step: Proton Donation from Water

TS3 (transition state 3), shown in Figure 9, is the TS of the third step. This TS is for the proton donation from H_2O to the C_α atom of IC2. The $H_2PO_4^-$ ion produced in the first step remains bound to the enolate intermediate in this step. In TS3, the distance of the breaking O–H bond is 1.266 Å, while the distance of the forming C_α–H bond is 1.347 Å. The local energy barrier of the third step is 28.4 kJ mol^{-1}, and the overall reaction barrier from the RC is 89.9 kJ mol^{-1}. This value is consistent with a slow reaction occurring in vivo, suggesting that the present reaction pathway actually operates in vivo.

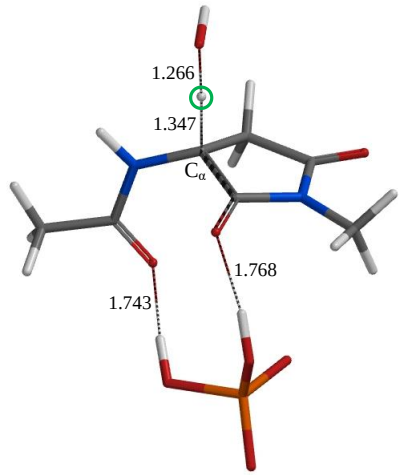

Figure 9: The geometry of TS3 (transition state 3) (φ = −57°, ψ = 150°) connecting IC2 (Figure 8) and the PC (Figure 10). Relevant interatomic distances are shown in Å. Grey: carbon; white: hydrogen; blue: nitrogen; red: oxygen; and orange: phosphorus. The transferring proton is indicated by the green circle.

Figure 10 shows the product complex (PC), which is a complex of the product (P), an $H_2PO_4^-$ ion, and an OH^- ion. P is the D-form of the model molecule and has the *syn*-periplanar conformation (the H_α–C_α–N–H dihedral angle is 11°). The hydrogen atom of the OH^- ion interacts with the nitrogen atom of the succinimide ring (2.622 Å). The relative energy of the PC with respect to the RC is high (63.5 kJ mol^{-1}). This is because P is complexed with an $H_2PO_4^-$ ion and an OH^- ion, instead of an

HPO_4^{2-} ion and an H_2O molecule. In order to confirm this, the geometries of the P·H_2O complex and the HPO_4^{2-} ion were separately optimized. The sum of the energies of these two species was comparable with the sum of the energies of the R·H_2O complex and the HPO_4^{2-} ion (Figure 3). Therefore, a complete low-energy pathway, which converts R (L-form) to P (D-form), has been found, and the HPO_4^{2-} ion is a strong candidate for being the in vivo catalyst of the stereoinversion of the succinimide intermediate formed in proteins and peptides.

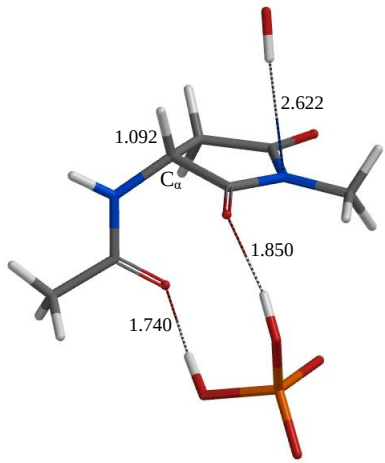

Figure 10: The geometry of the PC (product complex) (φ = −51°, ψ = 139°). Relevant interatomic distances are shown in Å. Grey: carbon; white: hydrogen; blue: nitrogen; red: oxygen; and orange: phosphorus.

3.4. Unsymmetrical S_E1 Mechanism (Pseudo-S_E2 Mechanism)

The most striking feature of the presently found mechanism of the succinimide stereoinversion is that the $H_2PO_4^-$ ion produced in the first step (the proton abstraction) remains bound until the stereoinversion is completed. In order to show the importance of this feature, the energy required for the removal of the $H_2PO_4^-$ ion from IC2 was calculated by optimizing the geometries of the enolate·H_2O complex and the $H_2PO_4^-$ ion separately. The sum of the energies of these two species was higher than IC2 by 33.2 kJ mol^{-1} (94.7 kJ mol^{-1} relative to the RC, see Figure 3). This

means that the conversion of IC2 to the PC via TS3 is more favored than the removal of the $H_2PO_4^-$ ion from IC2. Therefore, the $H_2PO_4^-$ ion is responsible for the low activation barrier associated with TS3. It is interesting to note that, in IC2, two anions (enolate and $H_2PO_4^-$) are bound together. Recently, attractive anion–anion interactions have received great interest [50], and the nature of the enolate–$H_2PO_4^-$ complex is to be clarified in the near future.

The enolate ion in IC2 has a flat structure because the C_α atom is sp^2-hybridized. However, because one side of the enolate plane is occupied by an $H_2PO_4^-$ ion, the reprotonation by water occurs on only one side of the enolate plane. The enolate intermediate is not symmetrically solvated.

The presently found stereoinversion mechanism may be regarded as an example of the S_E1 (substitution, electrophilic, and unimolecular) mechanism in that it involves a flat resonance-stabilized enolate ion intermediate [34–43]. The S_E1 mechanism is analogous to the well-known S_N1 (substitution, nucleophilic, and unimolecular) mechanism for nucleophilic substitution. In the S_E1 mechanism, the proton abstraction from the asymmetric carbon atom is postulated to be the rate-determining step [34–36,41–43]. Furthermore, it is often postulated that the enolate ion is equally solvated on both sides of the enolate plane and, hence, proton donation from the water solvent to the flat anionic intermediate occurs on either side of the plane [35,36,39–43]. In the present mechanism, however, these are not the case. The rate-determining step is not the first proton abstraction step, but the reprotonation of the enolate intermediate. Proton donation to the enolate intermediate from water occurs on only one side of the enolate plane, because the other side is blocked by an $H_2PO_4^-$ ion. Therefore, the stereoinversion mechanism found in this study may be termed an "unsymmetrical S_E1" mechanism.

As seen in Figure 3, the energy of TS3 is much higher than TS1 and the intermediate region is very flat. Therefore, the overall reaction can not be kinetically distinguished from a one-step reaction without any intermediates. This corresponds to the

push–pull-type S_E2 (substitution, electrophilic, and bimolecular) (S_E2 back) mechanism [34,36,38–43], which is an analogy of the S_N2 (substitution, nucleophilic, and bimolecular) mechanism for nucleophilic substitution. Therefore, the present mechanism may also be termed a "pseudo-S_E2" mechanism.

4. Conclusions

A low-energy HPO_4^{2-}-catalyzed reaction pathway was computationally found for the succinimide stereoinversion. The calculated activation barrier (ca. 90 kJ mol^{-1}) is consistent with a slow in vivo reaction, and the found mechanism may operate in long-lived proteins and peptides. The reaction proceeds in three steps. The first step is the proton abstraction from the C_α atom by the HPO_4^{2-} ion. The second step is a hydrogen bond rearrangement in the enolate intermediate complex produced in the first step. The third step is a proton donation from water to C_α, and this step is predicted to be the rate-determining step.

The proton donation in the third step occurs while the $H_2PO_4^-$ ion produced in the first step remains bound to the enolate intermediate. Therefore, the two sides of the enolate plane are not symmetrical, although the enolate has a flat geometry. The presently found novel mechanism can be termed the "unsymmetrical S_E1" or "pseudo-S_E2" mechanism.

We can expect the possibility that the HPO_4^{2-} ion also acts as a catalyst for other "undesired" nonenzymatic reactions in proteins and peptides related to aging and diseases. This should be addressed in future work. Moreover, the generality of the unsymmetrical S_E1 (pseudo-S_E2) mechanism also needs to be clarified in future work.

References

1. Cloos PAC, Christgau S. Non-enzymatic covalent modifications of proteins: Mechanisms, physiological consequences and clinical applications. Matrix Biol. 2002; 21: 39–52.
2. Hipkiss AR. Non-oxidative modification of DNA and proteins. In *Aging at the Molecular Level*; von Zglinicki, T., Ed.; Kluwer Academic Publishers: Dordrecht, The Netherlands. 2003; 145–177.
3. Cloos PAC, Christgau S. Post-translational modifications of proteins: Implications for aging, antigen recognition, and autoimmunity. Biogerontology. 2004; 5: 139–158.
4. Hipkiss AR. Accumulation of altered proteins and ageing: Causes and effects. Exp. Gerontol. 2006; 41: 464–473.
5. Truscott RJW. Are ancient proteins responsible for the age-related decline in health and fitness? Rejuvenation Res. 2010; 13: 83–89.
6. Truscott RJW, Friedrich MG. The etiology of human age-related cataract. Proteins don't last forever. Biochim. Biophys. Acta Gen. Subj. 2016; 1860: 192–198.
7. Truscott RJW, Schey KL, Friedrich MG. Old proteins in man: A field in its infancy. Trends Biochem. Sci. 2016; 41: 654–664.
8. Takahashi O, Kirikoshi R, Manabe N. Racemization of serine residues catalyzed by dihydrogen phosphate ion: A computational study. Catalysts. 2017; 7: 363.
9. Truscott RJW, Friedrich MG. Molecular processes implicated in human age-related nuclear cataract. Investig. Ophthalmol. Vis. Sci. 2019; 60: 5007–5021.
10. Friedrich MG. Spontaneous breakdown of long-lived proteins in aging and their implications in disease. In *Long-Lived Proteins in Human Aging and Disease*; Truscott, R.J.W., Ed.; Wiley-VCH GmbH: Weinheim, Germany. 2021; 97–125.
11. Ritz-Timme S, Collins MJ. Racemization of aspartic acid in human proteins. Ageing Res. Rev. 2002; 1: 43–59.
12. Ritz-Timme S, Laumeier I, Collins MJ. Aspartic acid racemization: Evidence for marked longevity of elastin in human skin. Br. J. Dermatol. 2003; 149: 951–959.

13. Fujii N, Saito T. Homochirality and life. Chem. Rec. 2004; 4: 267–278.
14. Fujii N. D-Amino acid in elderly tissues. Biol. Pharm. Bull. 2005; 28: 1585–1589.
15. Fujii N, Kaji Y, Fujii N. D-Amino acids in aged proteins: Analysis and biological relevance. J. Chromatogr. B 2011; 879: 3141–3147.
16. Fujii N, Takata T, Fujii N. Quantitative analysis of isomeric (L-α-, L-β-, D-α-, D-β-) aspartyl residues in proteins from elderly donors. J. Pharm. Biomed. Anal. 2015; 116: 25–33.
17. Fujii N, Takata T, Fujii N, Aki K, Sakaue H. D-Amino acid residues in proteins related to aging and age-related diseases and a new analysis of the isomers in proteins. In *D-Amino Acids: Physiology, Metabolism, and Application*; Yoshimura, T., Nishikawa, T., Homma, H., Eds.; Springer: Tokyo, Japan. 2016; 241–254.
18. Fujii N, Fujii N, Takata T, Sakaue H. The importance of the idea of "parachirality" in life science. In *Advances in Asymmetric Autocatalysis and Related Topics*; Pályi, G., Kurdi, R., Zucchi, C., Eds.; Academic Press: London, UK. 2017; 119–131.
19. Fujii N, Takata T, Fujii N, Aki K, Sakaue H. D-Amino acids in protein: The mirror of life as a molecular index of aging. Biochim. Biophys. Acta Proteins Proteom. 2018; 1866: 840–847.
20. Dyakin VV, Wisniewski TM, Lajtha A. Racemization in post-translational modifications relevance to protein aging, aggregation and neurodegeneration: Tip of the iceberg. Symmetry. 2021; 13: 455.
21. Morvan M, Mikšík I. Recent advances in chiral analysis of proteins and peptides. Separations. 2021; 8: 112.
22. Geiger T, Clarke S. Deamidation, isomerization, and racemization at asparaginyl and aspartyl residues in peptides. Succinimide-linked reactions that contribute to protein degradation. J. Biol. Chem. 1987; 262: 785–794.
23. Stephenson RC, Clarke S. Succinimide formation from aspartyl and asparaginyl peptides as a model for the spontaneous degradation of proteins. J. Biol. Chem. 1989; 264: 6164–6170.

24. Radkiewicz JL, Zipse H, Clarke S, Houk KN. Accelerated racemization of aspartic acid and asparagine residues via succinimide intermediates: An ab initio theoretical exploration of mechanism. J. Am. Chem. Soc. 1996; 118: 9148–9155.
25. Collins MJ, Waite ER, van Duin ACT. Predicting protein decomposition: The case of aspartic-acid racemization kinetics. Philos. Trans. R. Soc. Lond. B 1999; 354: 51–64.
26. Aki K, Fujii N, Fujii N. Kinetics of isomerization and inversion of aspartate 58 of αA-crystallin peptide mimics under physiological conditions. PLoS ONE. 2013; 8: e58515.
27. Takahashi O, Kirikoshi R, Manabe N. Racemization of the succinimide intermediate formed in proteins and peptides: A computational study of the mechanism catalyzed by dihydrogen phosphate ion. Int. J. Mol. Sci. 2016; 17: 16-98.
28. Sakaue H, Takata T, Fujii N, Sasaki H, Fujii N. Alpha B- and βA3-crystallins containing D-aspartic acids exist in a monomeric state. Biochim. Biophys. Acta Proteins Proteom. 2015; 1854: 1–9.
29. Sakaue H, Kinouchi T, Fujii N, Takata T, Fujii N. Isomeric replacement of a single aspartic acid induces a marked change in protein function: The example of ribonuclease A. ACS Omega. 2017; 2: 260–267.
30. Fujii N, Takata T, Kim I, Morishima K, Inoue R, et al. Asp isomerization increases aggregation of α-crystallin and decreases its chaperone activity in human lens of various ages. Biochim. Biophys. Acta Proteins Proteom. 2020; 1868: 140446.
31. Robinson NE, Robinson AB. *Molecular Clocks: Deamidation of Asparaginyl and Glutaminyl Residues in Peptides and Proteins*; Althouse Press: Cave Junction, OR, USA. 2004.
32. Dudley KH, Bius DL. Buffer catalysis of the racemization reaction of some 5-phenylhydantoins and its relation to the in vivo metabolism of ethotoin. Drug Metabol. Dispos. 1976; 4: 340–348.
33. Voet D, Voet JG. *Biochemistry*, 4th ed.; John Wiley & Sons, Inc.: Hoboken, NJ, USA. 2011; 45–69.

34. Abraham MH. Mechanisms of electrophilic substitution at saturated carbon. In *Comprehensive Chemical Kinetics*; Bamford CH, Tipper CFH, Eds, Elsevier: Amsterdam, The Netherlands. 1973; 12: 11–21.
35. Reist M, Christiansen LH, Christoffersen P, Carrupt PA, Testa B. Low configurational stability of amfepramone and cathinone: Mechanism and kinetics of chiral inversion. Chirality. 1995; 7: 469–473.
36. Reist M, Carrupt PA, Testa B, Lehmann S, Hansen JJ. Kinetics and mechanisms of racemization: 5-substituted hydantoins (= imidazolidine-2,4-dions) as models of chiral drugs. Helv. Chim. Acta. 1996; 79: 767–778.
37. Mey B, Paulus H, Lamparter E, Blaschke G. Kinetics of racemization of (+)- and (−)-diethylpropion: Studies in aqueous solution, with and without the addition of cyclodextrins, in organic solvents and human plasma. Chirality. 1998; 10: 307–315.
38. Kahn K, Tipson PA. Kinetics and mechanism of allantoin racemization. Bioorg. Chem. 2000; 27: 62–72.
39. Reist M, Testa B, Carrupt PA. Drug racemization and its significance in pharmaceutical research. In *Stereochemical Aspects of Drug Action and Disposition*; Eichelbaum, M., Testa, B., Somogyi, A., Eds.; Springer: Berlin, Germany. 2003; 91–112.
40. Cabordery AC, Toussaint M, Azaroual N, Bonte JP, Melnyk P, et al. Kinetics and mechanism of racemization of Tic-hydantoins, potent sigma-1 agonists. Tetrahedron Asymmetry. 2011; 22: 125–133.
41. Ahmad HO. Kinetics and Mechanism of Racemization Reactions of Configurationally Liable Stereogenic Centers in Drug-Like Molecules in Aqueous Solutions; Thiohydantoins and Related Compounds. Ph.D. Thesis, Cardiff University, Cardiff, UK, 2015.
42. Dalal M. *A Textbook of Organic Chemistry-Volume I*; Dalal Institute: Rohtak, India. 2019; 302–311.
43. Ballard A, Narduolo S, Ahmed HO, Keymer NI, Asaad N, et al. Racemisation in Chemistry and Biology. Chem. Eur. J. 2020; 26: 3661–3687.
44. *Spartan'20*, version 1.1.2; Wavefunction, Inc.: Irvine, CA, USA. 2021.

45. Chai JD, Head-Gordon M. Long-range corrected hybrid density functionals with damped atom–atom dispersion corrections. Phys. Chem. Chem. Phys. 2008; 10: 6615–6620.
46. Thanthiriwatte KS, Hohenstein EG, Burns LA, Sherrill CD. Assessment of the performance of DFT and DFT-D methods for describing distance dependence of hydrogen-bonded interactions. J. Chem. Theory Comput. 2011; 7: 88–96.
47. Demichelis R, Garcia NA, Raiteri P, Malini RI, Freeman CL, et al. Simulation of calcium phosphate species in aqueous solution: Force field derivation. J. Phys. Chem. B 2018; 122: 1471–1483.
48. Moser AT. Computational Investigation of Nucleic Acids. Ph.D. Thesis, University of Minnesota, Minneapolis, MN, USA, 2009.
49. Florián J, Warshel A. Langevin dipoles model for ab initio calculations of chemical processes in solution: Parametrization and application to hydration free energies of neutral and ionic solutes and conformational analysis in aqueous solution. J. Phys. Chem. B 1997; 101: 5583–5595.
50. Pizzi A, Dhaka A, Beccaria R, Resnati G. Anion···anion self-assembly under the control of σ- and π-hole bonds. Chem. Soc. Rev. 2024; 53: 6654–6674.